Nanoscale

COMMUNICATION

View Article Online
View Journal | View Issue

Cite this: *Nanoscale*, 2019, **11**, 418

Received 30th October 2018,
Accepted 26th November 2018

DOI: 10.1039/c8nr08728h

rsc.li/nanoscale

Modulated interlayer charge transfer dynamics in a monolayer TMD/metal junction†

Linglong Zhang, *‡[a,b] Han Yan,*‡[b] Xueqian Sun,*‡[b] Miheng Dong,[b] Tanju Yildirim,[b] Bowen Wang,[b] Bo Wen,[b] Guru Prakash Neupane,[b] Ankur Sharma,[b] Yi Zhu,[b] Jian Zhang,[b] Kun Liang,[b] Boqing Liu,[b] Hieu T. Nguyen,[b] Daniel Macdonald[b] and Yuerui Lu *[b]

The performance of optoelectronic devices based on monolayer transition-metal dichalcogenide (mTMD) semiconductors is significantly affected by the contact at the mTMD–metal interface, which is dependent on interlayer interactions and coupling. Here, we report a systematic optical method to investigate the interlayer charge transfer and coupling in a mTMD–metal heterojunction. Giant photoluminescence (PL) quenching was observed in a monolayer MoS_2/Pd (1L MoS_2/Pd) junction which is mainly due to the efficient interlayer charge transfer between Pd and MoS_2. 1L MoS_2/Pd also exhibits an increase in the PL quenching factor (η) as the temperature decreases, due to a reduction of the interlayer spacing. Annealing experiments were also performed which supported interlayer charge transfer as the main mechanism for the increase of η. Moreover, a monolayer MoS_2/Au (1L MoS_2/Au) junction was fabricated for engineering the interlayer charge transfer. Interestingly, a narrowing effect of the full width at half maximum (FWHM) was encountered as the junctions changed from 1L MoS_2/SiO_2 → 1L MoS_2/Au → 1L MoS_2/Pd, possibly originating from a change of the doping level induced weakening of exciton-carrier scattering. Our results deepen the understanding of metal–semiconductor junctions for further exploring fundamental phenomena and enabling high-performance devices using mTMD–metal junctions.

Metal–semiconductor junctions play an important role in optoelectronic and electronic devices. Monolayer transition-metal dichalcogenides (mTMDs) possessing an extremely small thickness (a few Å), a uniform band gap over a large range (1–2 eV) and a pristine interface without dangling bonds are important building blocks for metal–semiconductor junctions.[1–3] It is known that the van der Waals gap (vdW gap) (*i.e.*, interlayer spacing) at the interface between TMD and metal exists due to the lack of dangling bonds, and these dominate the interlayer interaction and coupling of mTMD–metal junctions.[4–6] Moreover, temperature could effectively modulate the interlayer interaction (*i.e.*, interlayer charge transfer) and coupling, attributed to temperature induced changes in the interlayer spacing.[4–6] To date, various monolayer TMDs have been integrated with multiple metals for fabricating metal–TMD junctions, which can enable the engineering of the interlayer interaction and coupling.[4–12] However, systematic studies of temperature-dependent interlayer spacing and interlayer charge transfer in metal–TMD interfaces have not been reported. Moreover, the previous research on the mTMD–metal junctions was generally conducted by electrical methods, which require a complicated fabrication and characterization process and which involve hard to avoid chemical contaminations.[4,7,10,12,13] In addition, it's important to explore the temperature induced phenomenon to distinguish the effects of other factors, such as substrate, interference, doping level change, *etc.*[4,6,14] Therefore, a simple optical method and comprehensive study of interlayer charge transfer and coupling in mTMD–metal junctions are critical for enabling various novel optoelectronic and electronic device designs.

Herein, we demonstrate a systematic optical method to study the interlayer charge transfer phenomenon in mTMD–metal junctions. Firstly, we transferred an exfoliated monolayer MoS_2 onto palladium (1L MoS_2/Pd) and observed significant photoluminescence (PL) quenching from the monolayer MoS_2 PL peak as compared with that of 1L MoS_2 on a SiO_2 (1L MoS_2/SiO_2) substrate. It is expected that the monolayer TMD on the metal substrate would lead to PL quenching, possibly due to additional nonradiative exciton recombination paths (*e.g.*, interlayer charge transfer).[14,15] Based on the PL quenching factor (η), we studied the interlayer charge transfer directly. Here, the higher the η, the higher the charge transfer

[a]*National Laboratory of Solid State Microstructures, Collaborative Innovation Center of Advanced Microstructures, School of Electronic Science and Engineering, Nanjing University, Nanjing 210093, People's Republic of China.*
E-mail: linglong.zhang@yahoo.com
[b]*Research School of Engineering, College of Engineering and Computer Science, the Australian National University, Canberra, ACT 2601, Australia.*
E-mail: yuerui.lu@anu.edu.au

†Electronic supplementary information (ESI) available. See DOI: 10.1039/c8nr08728h

‡These authors contributed equally to this work.

efficiency. To study the temperature-dependent interlayer charge transfer, variable PL measurements were conducted showing an increase in the η value with decreasing temperature. Ultra-high charge transfer efficiency was observed in the 1L MoS_2/Pd junction at 83 K. This is mainly ascribed to the decrease in temperature induced interlayer spacing reduction and this results in highly efficient interlayer charger transfer.[2,3,6,16] Additionally, annealing experiments were performed which further provided evidence that decreasing interlayer spacing dominates the PL quenching phenomena. Moreover, a monolayer MoS_2 on a Au (1L MoS_2/Au) junction was fabricated to further explore the material related interlayer charge transfer. It also shows a similar increasing tendency of η as the temperature decreases. In addition, there is a narrowing of the full width at half maximum (FWHM) according to 1L MoS_2/SiO_2 → 1L MoS_2/Au → 1L MoS_2/Pd and this is possibly due to the changed doping levels induced by a change of exciton-carrier scattering. Furthermore, we quantitatively estimated the doping level of 1L MoS_2 in the three junctions *via* a mass action model within the three-level model framework, suggesting that Pd induced the highest level of P-doping. Our findings provide a simple and effective optical method to study mTMD–metal junctions and the corresponding doping level of a mTMD; these results can enable various novel opto-electronic and electronic device designs based on 2D material–metal junctions.

In a mTMD–metal junction design, the relative band alignment is crucial to determine the doping behavior and charge transfer, and this depends on the work function potential of the metal and the Fermi-level pinning effect at the interface.[1,17] Fig. 1a and b show the alignment of the monolayer MoS_2 and Pd's work function before contact and after

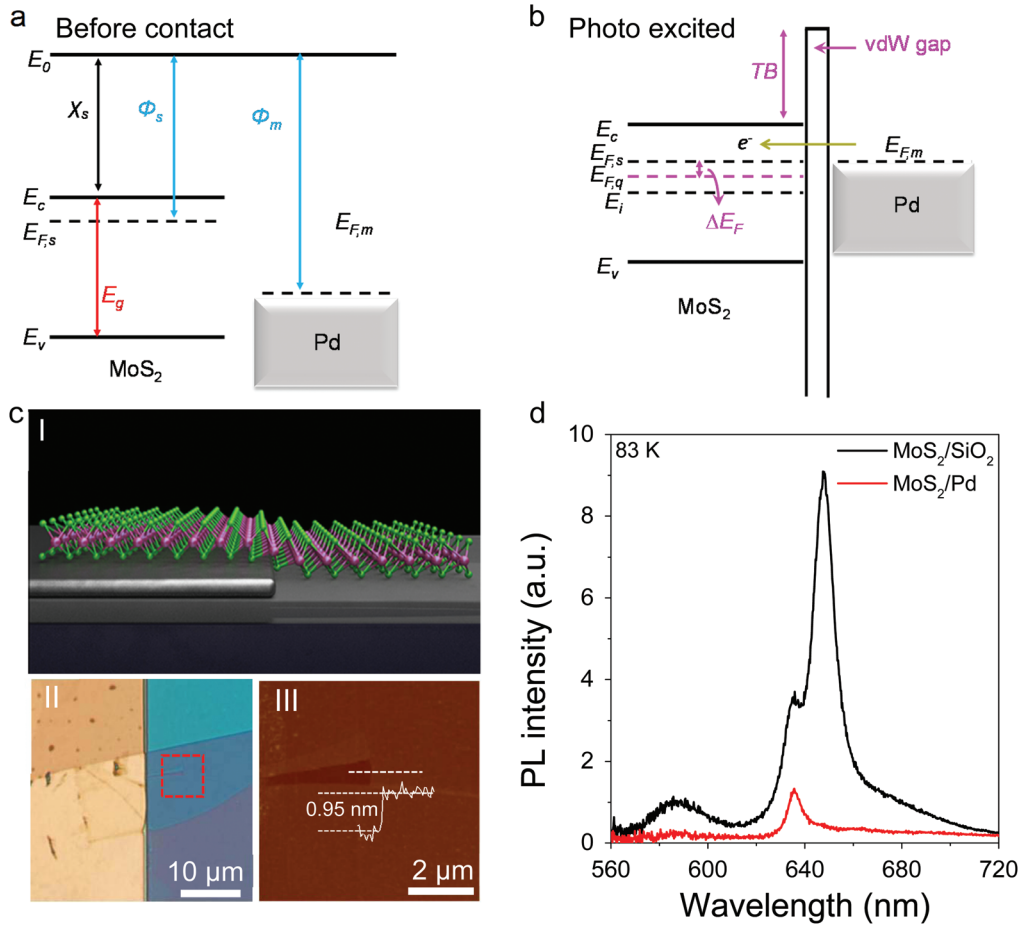

Fig. 1 Demonstration of interlayer charge transfer. (a) Band alignment before metal–semiconductor formation showing the intrinsic doping of 1L MoS_2. E_0, χ_s, and E_c represent the vacuum level, electron affinity energy, and conduction band, respectively. $E_{F,s}$, E_v, and E_g represent the Fermi level of 1L MoS_2, valence band and band gap, respectively. ϕ_s, ϕ_m, and $E_{F,m}$ represent the work function of 1L MoS_2 and Pd and the Fermi level of Pd, respectively. (b) The band alignment after the formation of the metal–semiconductor junction during the photoexcited process showing the photo-excited induced doping level of 1L MoS_2. E_c, $E_{F,s}$, and $E_{F,q}$ represent the conduction band, Fermi level of monolayer MoS_2, and dynamic equilibrium state Fermi level of monolayer MoS_2 with photoexcitation, respectively. E_i, E_v, ΔE_F, TB and $E_{F,m}$ represent the Fermi level of the electrical neutrality state, valence band, photoexcitation-induced Fermi level shift, tunneling barrier height and Fermi level of Pd. (c) ((I), (II)) Schematic (I) and the corresponding optical image (II) after monolayer MoS_2 transferred on Pd showing MoS_2/Pd and MoS_2/SiO_2 regions. Scale bar, 10 μm. (III) AFM image of the dotted rectangular area shown in (II). Inset: height measurements along the dashed line showing the atomic layer thickness. (d) PL spectra of 1L MoS_2/SiO_2 and 1L MoS_2/Pd junctions at 83 K showing giant PL quenching.

contact.[1,7,17] After the junctions are formed, the Fermi level ($E_{F,s}$) position shifts towards the middle band gap (E_i) of MoS_2 and then reaches an equilibrium, in which both the Pd and mTMD share the same Fermi level due to contact doping and the Fermi pining effect.[1,17] As shown in Fig. 1b, the Fermi level position ($E_{F,s}$) indicates that the 1L MoS_2/Pd junction is still n-type after the Pd induced P doping, consistent with previous experiments and theoretical predictions.[5,7,17] In the PL measurements, photo-excited carriers would further shift the Fermi level of 1L MoS_2 towards E_i reaching a new quasi-fermi level ($E_{F,q}$). The dynamic equilibrium Fermi level difference (ΔE_F) is equal to the applied voltage and this leads to multiple electrons transferring from the metal to the interface (*i.e.*, interlayer charge transfer) (Fig. 1b).[18–20] Therefore, based on the fast interfacial charge transfer between Pd and 1L MoS_2,[21,22] photo-excited holes would be annihilated at the interface by the electrons from Pd and this results in PL quenching of 1L MoS_2 in a 1L MoS_2/Pd junction.[22,23]

Fig. 1c shows the bottom-contact monolayer MoS_2/Pd (1L MoS_2/Pd) junction in order to substantiate the above interlayer charge transfer mechanism (Fig. 1c). The top (I) and bottom left (II) parts in Fig. 1c show the schematic and optical image of the 1L MoS_2/Pd junction. The 1L MoS_2/Pd junction was prepared *via* transferring mechanically exfoliated 1L MoS_2 over patterned 50 nm thick Pd electrodes that were deposited onto a 260 nm Si/SiO_2 substrate. Based on this dry-transfer method, a 1L MoS_2/SiO_2 region could also be simultaneously achieved.[24] This is an effective way to avoid contamination, helping to achieve ultra-clean and intact interfaces.[25,26] After the formation of the junction, the 1L MoS_2/Pd and 1L MoS_2/SiO_2 junctions were characterized by Raman spectroscopy to confirm the individual thickness and interfaces (Fig. S1†). AFM microscopy (Fig. 1c (III)) and phase-shift interferometry (PSI) images (Fig. S2, S3 and ESI note S1†) also confirmed the presence of monolayer MoS_2.[22] PL spectroscopy is a powerful tool to study the dynamic interlayer and intralayer charge transfer excitonic states and this can provide the evidence for interlayer charge transfer and coupling in the junction constituent layers.[25,27,28] Moreover, the low temperature influences trion emissions in the spectra and PL intensity.[24,29] Thus, the PL spectra of the 1L MoS_2/Pd and 1L MoS_2/SiO_2 junctions were recorded at 83 K, exhibiting three peaks around 587, 634 and 648 nm, which are assigned to B exciton, A exciton and A^- trion, respectively (Fig. 1d).[30,31] The PL intensity (sum of B exciton, A exciton and A^- peak) of the 1L MoS_2/Pd junction demonstrates giant quenching (~9.7 times) compared to the 1L MoS_2/SiO_2 junction, suggesting that highly efficient interlayer charge transfer had occurred. Several similar devices (>6) of 1L MoS_2/Pd and 1L MoS_2/SiO_2 showed repeatable results. Additionally, a consistent quenching factor was measured in the device two months after fabrication, demonstrating the stability in the mTMD–metal junction.

Tight-binding or quantum tunneling mode interlayer interaction and coupling properties are highly related to the interlayer spacing and are heavily dependent on temperature.[2,3,6] Thus, in order to substantiate that the interlayer charge transfer mainly affects the PL quenching, variable-temperature PL measurements were conducted in the temperature range from 298 K to 83 K (Fig. 2a).[6] For comparison, the PL spectra of 1L MoS_2/SiO_2 are also presented. In Fig. 2a, both PL peaks exhibit a blue shift with decreasing temperature similar to earlier findings.[30,31] In contrast to PL peak shape from the 1L MoS_2/SiO_2 junction at each temperature, the 1L MoS_2/Pd junction indicated an A exciton dominant peak, which suggests the lower n type level of monolayer MoS_2 in the 1L MoS_2/Pd junction and this is ascribed to the Pd induced high P doping effect and Fermi level pinning effect.[1,5,12,32] Fig. 2b shows the temperature dependent quenching factor (η), where the quenching factor η is defined as the ratio of the integrated PL intensity (sum of B exciton, A exciton and A^- peak) in 1L MoS_2/SiO_2 to that of the 1L MoS_2/Pd junction (*i.e.*, $\eta = I_{MoS_2}/I_j$). As shown in Fig. 2b, η increases monotonically from 2.6 to 9.7 as the temperature decreases from 298 K to 83 K. This suggests that lower temperature induced interlayer spacing reduction promotes a more efficient interlayer charge transfer.[1,6] Specifically, as the temperature decreases, the anharmonicity leads to a contraction of the interlayer spacing in the 1L MoS_2/Pd junction, which in turn, enhances interlayer interaction inducing a larger η and a stronger coupling effect.[6,33] Hence, the large change of the quenching factor as a function of the temperature illustrates that the interlayer charge transfer is the dominant factor in the PL quenching phenomena, rather than the other factors such as substrate, absorption, scattering, surface quality, doping level effects, *etc*.[6] This is because the doping level of monolayer MoS_2 on the two substrates (*i.e.*, Pd and SiO_2) only changes slightly due to a change in temperature; the quenching factor should have less variation with the change in temperature. On the other hand, if we assume that the substrate, absorption and scattering play a bigger role in PL quenching compared to other factors, the quenching factor should be nearly independent of the temperature. However, this was not observed in the PL measurements which implies the significant importance of the reduction in the interlayer spacing. In addition, the quenching factor was fitted well by the empirical equation which only considered interlayer spacing effects, further supporting our arguments (ESI note S2†).[6] It is also expected that the annealing process decreases the interlayer spacing and thus higher interlayer charge transfer efficiency occurs since annealing drives out trapped residual molecules within the junction.[6,34] Therefore, the 1L MoS_2/Pd junction was annealed at 573 K for 30 min after the variable temperature measurements.[34] Afterwards, the room-temperature PL measurements were performed again after the sample cooled down from high temperature in order to make comparisons due to annealing effects (Fig. 2c and S4†). Also, the corresponding AFM images before and after the annealing of 1L MoS_2 onto Pd are displayed as a reference (Fig. S4b†). As shown in Fig. S4,† the PL spectral shape of both junctions did not show a significant change as compared to before the annealing process, suggesting that this annealing process did not influence the doping level of MoS_2 too much. It is also worth noting that larger PL quenching (~10.3 times) was exhibited when com-

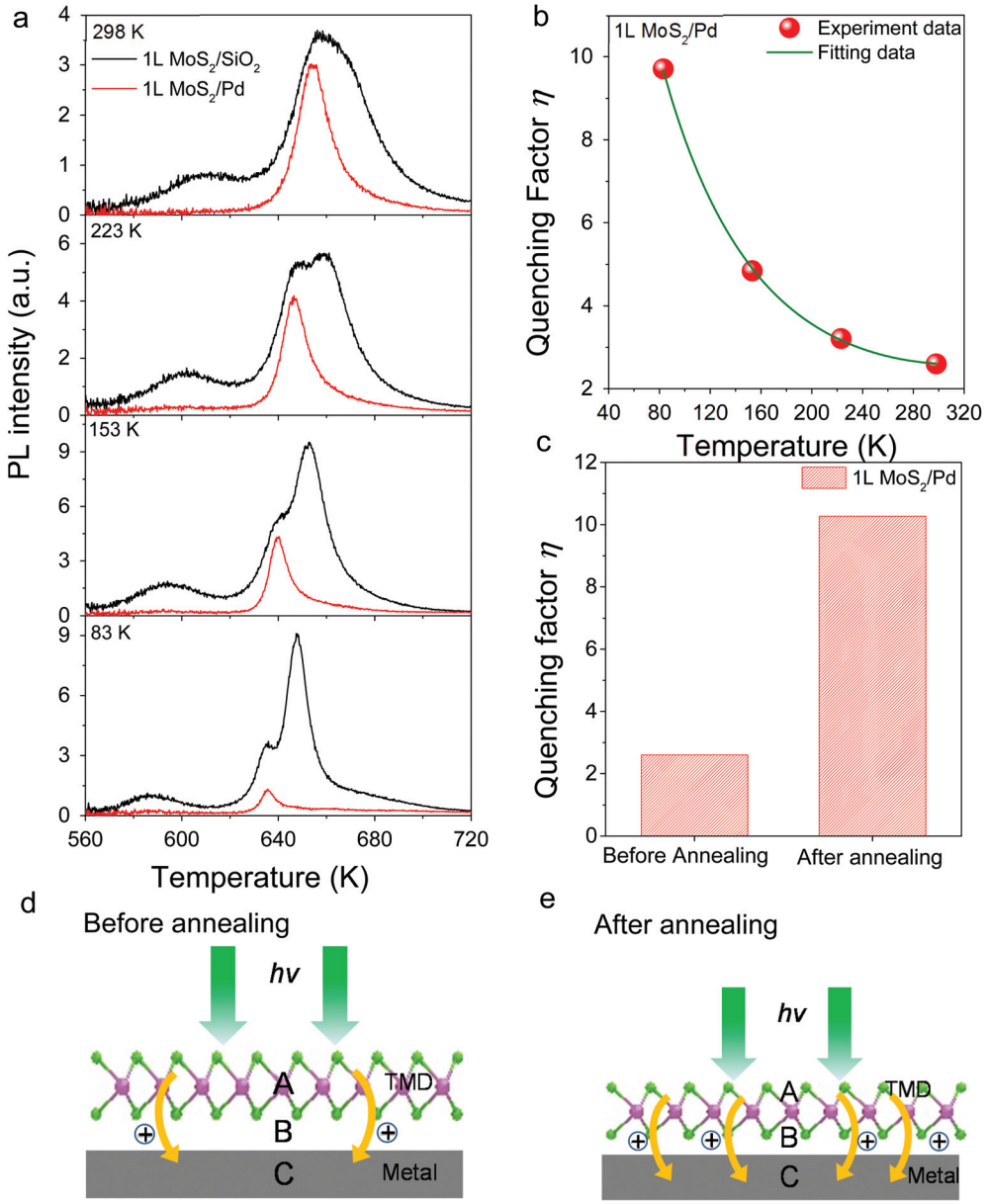

Fig. 2 Temperature-dependent interlayer charge transfer. (a) PL spectra of the 1L MoS_2/Pd structure and 1L MoS_2 as a function of temperature. The black and red solid lines denote the experimental data from the heterostructures of 1L MoS_2/Pd and 1L MoS_2/SiO_2, respectively. (b) PL quenching factors (η) *versus* temperature curve in the 1L MoS_2/Pd structure. The red balls represent the measured η value as a function of temperature. The olive line denotes the fitting curve, which suggests that the interlayer charge transfer is dominant in the quenching factor variation due to the temperature induced interlayer spacing change. (c) Room-temperature PL quenching factor histogram in the 1L MoS_2/Pd junction before and after the annealing process. The annealing process was conducted at 573 K for 30 min. (d) Schematic diagram of the 1L MoS_2/Pd junction shows charge transfer efficiency before annealing where the larger interlayer spacing indicates lower charge transfer efficiency. (e) Schematic diagram of the 1L MoS_2/Pd junction shows charge transfer efficiency before annealing. As compared with that in (d), the smaller interlayer spacing indicates higher charge transfer efficiency.

pared to before annealing (2.6 times) (Fig. 2c). Furthermore, Fig. 2d and e show the schematic of the mTMD–metal junction before and after the annealing process, respectively, during the photoexcitation process.[1,6,34] This demonstrates that the interlayer spacing decreases *via* an annealing process, leading to an increased interlayer charge transfer efficiency and thus a higher PL quenching factor and higher coupling effect.

In a 2D TMD/metal junction, the interlayer charge transfer and coupling is also sensitive to the constituent materials of the junction.[1,6] To explore how different junction materials engineer the interlayer charge transfer, a 1L MoS_2/Au junction was fabricated as shown in Fig. 3a. The corresponding characterization was conducted to confirm the formation of individual interfaces (Fig. S2 and S5†).[22] Similar to the 1L MoS_2/Pd junction,

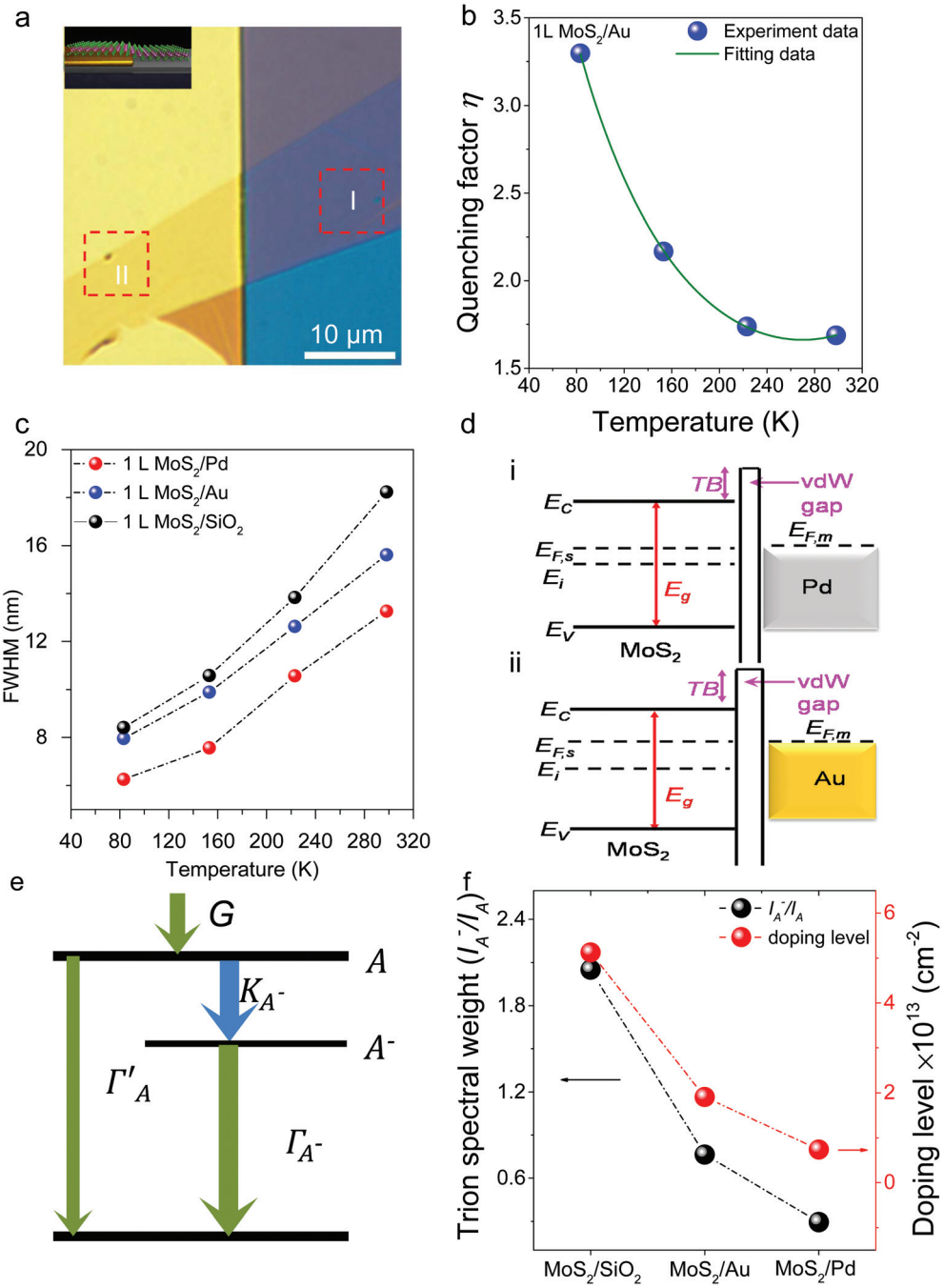

Fig. 3 Material-dependent interlayer charge transfer. (a) Optical image of 1L MoS_2 transferred onto Au showing MoS_2/Au and MoS_2/SiO_2 regions. Scale bar, 10 μm. Inset: Schematic of the 1L MoS_2/Au structure. (b) PL quenching factors (η) *versus* temperature curve in the 1L MoS_2/Au structure. Blue balls denote the PL quenching factor as a function of temperature. The olive line represents the fitting curve. (c) FWHM of three junctions, such as 1L MoS_2/Pd, 1L MoS_2/Au and 1L MoS_2/SiO_2, as a function of temperature. (d) Band alignments after the formations of (i) the 1L MoS_2/Pd junction and (ii) the 1L MoS_2/Au junction. This shows the doping level of 1L MoS_2 onto the metal substrate. Here, 1L MoS_2 in the 1L MoS_2/Pd junction shows the more neutral state, compared with the 1L MoS_2/Au junction, which implies that the equilibrium Fermi level would move more towards to the gap middle in the 1L MoS_2/Pd junction. (e) Three level energy diagram exhibiting the exciton (A), trion (A^-), and ground state. (f) Trion spectra weight (left) and the doping level (right) of 1L MoS_2 as a function of various junctions, such as 1L MoS_2/SiO_2, 1L MoS_2/Au and 1L MoS_2/Pd.

the 1L MoS_2/Au junction also displayed an increase in the quenching factor with decreasing temperature (Fig. 3b). This result manifested that the interlayer spacing plays a crucial role in the interlayer charge transfer. Also, the corresponding characterization of MoS_2 thickness-dependent heterostructures are presented as a reference and shows a similar tendency after the annealing process (Fig. S6†). In addition, 1L WSe_2/Au and 1L WSe_2/SiO_2 junctions were characterized as a

reference and indicated similar observations with MoS_2 based junctions (Fig. S7†). Moreover, the 1L MoS_2/Au junction has a smaller quenching factor than the 1L MoS_2/Pd junction at each temperature, possibly due to the smaller interlayer spacing and the lack of orbital overlaps in the former.[1,35] The doping level and substrate effects on the quenching factor can be the subject of investigation in future topics. Correspondingly, the empirical equation in ESI note S2,† which only considered the interlayer spacing effects, was applied to fit the quenching factor in Fig. 3b and this suggests again that interlayer spacing dominates the quenching factor. Fig. 3c shows the A exciton FWHM of three junctions as a function of the temperature. For the three junctions, as the temperature decreases, the A exciton FWHM decreases accordingly and this is consistent with earlier reports (detailed in ESI note S3†).[14,15,36] Interestingly, it was observed that at each temperature, the A exciton FWHM of the three junctions has the following ranking: 1L MoS_2/SiO_2 > 1L MoS_2/Au > 1L MoS_2/Pd. The possible reason for the narrowing effect of the A exciton FWHM is due to the doping-related weakening of exciton-carrier scattering.[14,15] In Fig. 3d, the relative band alignments of both junctions were plotted, denoting n-type behavior. Compared to the 1L MoS_2/Pd junction, the lower work function (WF) of Au in a 1L MoS_2/Au junction could lead to lower P doping in monolayer MoS_2 which has been reported in previous theoretical studies and experiments.[1,7,17] Moreover, gate-dependent PL measurements were performed at room temperature and at 83 K (Fig. S8†), consistent with earlier reports.[30,31] For quantitative comparisons, the temperature-dependent PL spectra of 1L MoS_2/Pd and 1L MoS_2/Au were fitted by Lorentz fitting (Fig. S9†). Meanwhile, Fig. S10† presents the fitting of gate-dependent PL spectra at 83 K and temperature-dependent PL spectra from 1L MoS_2 on SiO_2. The 1L MoS_2/Au junction displayed prominent trion peaks, especially at 83 K, supporting again that the Au contact produces lower level P doping at the MoS_2 interface (Fig. S9†).[30] Furthermore, for the quantitative analysis of the doping behavior of the three junctions, the excited dynamics has been studied *via* a three-level model, where the trion, exciton and ground state were included (Fig. 3e). Here, G, Γ_A and Γ_{A^-} denote the A exciton generation rate, A exciton decay rate and trion decay rate, respectively. We claim that Γ_A could be decomposed into two parts, which are the exciton rate without including the trion formation (Γ'_A) and trion formation rate (K_{A^-}). Then the PL intensity of exciton (I_A) and trion (I_{A^-}) from the different junctions could be estimated within the framework of a three-level model under steady-state conditions (ESI note S4†). Based on the PL spectral fittings in Fig. S7 and S8,† the trion spectral weight (I_{A^-}/I_A) is presented in Fig. 3f. It shows a decreasing trend of trion spectral weight when the junctions change from 1L MoS_2/SiO_2 → 1L MoS_2/Au → 1L MoS_2/Pd. In particular, 1L MoS_2/SiO_2 and 1L MoS_2/Pd have an I_{A^-}/I_A value of 2.05 and 0.29, respectively. This suggests that the n type level among the three junctions has the same tendency: 1L MoS_2/SiO_2 > 1L MoS_2/Au > 1L MoS_2/Pd, which is consistent with earlier findings.[1,5,7,30,31] Furthermore, according to the mass action model, the junction material dependent doping level is shown in Fig. 3f (detailed in ESI note S4†). This indicates that the 1L MoS_2/SiO_2, 1L MoS_2/Au and 1L MoS_2/Pd junctions have an electron density value of 5.1×10^{13}, 1.9×10^{13} and 7.4×10^{12} cm^{-2}, respectively. Thus, the 1L MoS_2/Au and 1L MoS_2/Pd junctions exhibited a doping reduction rate of 63 and 86%, respectively, consistent with theoretical predictions.[1,5,15,35]

Based on the above analysis, and in contrast with the 1L MoS_2/SiO_2 junction, the PL intensity of mTMD–metal junctions, such as 1L MoS_2/Pd and 1L MoS_2/Au, is enhanced since the n type level of monolayer MoS_2 on the metal (*e.g.*, Pd and Au) significantly decreases, whereas the doping level induced PL increasing phenomenon was not observed in experiments and this reflects that doping is not responsible for PL quenching. This also implies that the interlayer charge transfer dominates PL quenching.[26,31,37] Lastly, to evaluate the contribution of MoS_2 to the coupling properties of the different junctions, the A exciton peak energy as a function of temperature was fitted by the modified Varshni relationship given by (Fig. S11†):[36]

$$E(T) = E_0 - S\langle\hbar\omega\rangle\left[\cot h\frac{\langle\hbar\omega\rangle}{2K_BT} - 1\right] \quad (1)$$

where E_0 is the emission energy at 0 K and S is the Huang–Rhys factor, representing the strength of exciton–phonon coupling. The higher the S, the stronger the exciton–phonon coupling.[6] $\langle\hbar\omega\rangle$ is the average photon energy. By comparing the exciton–phonon coupling (S) among the junctions, the contribution of monolayer MoS_2 to the interlayer coupling has the following order: 1L MoS_2/Pd > 1L MoS_2/Au (ESI S5 and Table S1†). Our results provide a simple way to precisely engineer the interlayer charge transfer in a mTMD–metal junction and this is important in understanding the fundamental phenomena of interlayer charge transfer and coupling properties that can enable advanced future optoelectronic devices.

In conclusion, a systematic optical method to investigate the interlayer charge transfer of mTMD–metal junctions that comprise of a monolayer MoS_2 and various metals (*e.g.*, Pd and Au) has been demonstrated. This provides a simple and powerful platform to explore interlayer charge transfer and coupling properties in the junctions. A giant PL quenching phenomenon was observed in a 1L MoS_2/Pd junction and this was due to highly efficient interlayer charge transfer. Moreover, the quenching factor (η) exhibits an increasing trend with reducing temperature. This also implies an increase in the interlayer charge transfer efficiency that is attributed to the temperature induced interlayer spacing reduction between the monolayer TMD and metal. Annealing experiments were also conducted in which an increase in the quenching factor η was observed; this result additionally provided evidence that the reduced interlayer spacing promotes interlayer charge transfer and an increase of η. In addition, we modulated the interlayer charge transfer by changing the junction materials (*i.e.*, 1L MoS_2/Au junction). A narrowing effect of the FWHM

was found as the junction changes from 1L MoS_2/SiO_2 → 1L MoS_2/Au → 1L MoS_2/Pd and this was possibly attributed to doping level related weakening of exciton-carrier scattering. Furthermore, the doping level of 1L MoS_2 from the three heterojunctions was qualitatively determined *via* the mass action model within a three-level model framework. Our demonstration highlights the significance of the temperature modulation of interlayer charge transfer and coupling in mTMD–metal junctions providing guidelines that are crucial for future novel optoelectronic designs and investigating fundamental phenomena in 2D TMD–metal junctions.

Experimental methods

Device fabrication and characterization

Patterned metal substrates were fabricated using electron beam lithography (EBL) on a SiO_2/Si substrate (260 nm thermal oxide on n^+-doped silicon). Then, monolayer TMD film materials were exfoliated *via* the Scotch tape method and transferred onto the designated substrate *via* the dry transfer method.[31] The monolayer TMD films were characterized by optical microscopy, AFM and Raman spectroscopy to identify the number of layers and topological information. For the MOS structures, used for back gate-dependent PL measurements, we transferred the 100 nm thick gold electrode to contact a part of the TMD flakes as the probing pad. For the thermal annealing process, the 1L MoS_2/Pd junction was kept in a Linkam THMS 600 chamber with a slow flow of N_2 gas for sample protection while being maintained at 573 K for 30 min.

Optical characterization

PL and Raman measurements were conducted using a Horiba LabRAM system equipped with a confocal microscope, a charge-coupled device (CCD) Si detector, and a 532 nm diode-pumped solid-state (DPSS) laser as the excitation source. If there is no special illustration, on-sample power is always 43.8 μW. For temperature-dependent (above 83 K) measurements, the sample was placed in a microscope-compatible chamber with a low-temperature controller (using liquid nitrogen as the coolant). Many samples (>6) have been measured for every single structure and the results are repeatable. The electrical bias was applied using a Keithley 4200 semiconductor analyzer. All the optical path length (OPL) characterization was obtained using a phase-shifting interferometer (Vecco NT9100).

Author contributions

L. L. Z., H. Y. and X. S. contributed equally to this work. Y. R. L. conceived and supervised the project; L. L. Z., X. S., and M. D. prepared the samples; H. T. N. and D. M. contributed to the PL experiments; L. L. Z. and H. Y. conducted the measurements; L. L. Z. and B. W. W. did the PSI measurements. B. W., Y. Z., A. S., T. Y., J. Z., K. L., B. L. and G. N. contributed to data analysis; L. L. Z., H. Y. and T. Y. co-wrote the paper; all authors discussed the results and commented on the manuscript.

Conflicts of interest

The authors declare that they have no competing financial interests.

Acknowledgements

We would like to acknowledge the facility support from Professor Chennupati Jagadish's group at the ANU, ACT node of the Australian National Fabrication Facility (ANFF). We also acknowledge financial support from the ANU Ph.D. student scholarship, the China Scholarship Council, the ANU Major Equipment Committee fund (No. 14MEC34), and the Australian Research Council (ARC) Discovery Early Career Researcher Award (DECRA) DE140100805. We further acknowledge ARC Discovery Project (DP180103238). H. T. N. acknowledges the fellowship support from the Australian Centre for Advanced Photovoltaics (ACAP).

References

1 J. Kang, W. Liu, D. Sarkar, D. Jena and K. Banerjee, *Phys. Rev. X*, 2014, **4**, 031005.
2 P. L. Walker, H. A. M. Jr. and C. C. Wright, *Ind. Eng. Chem.*, 1953, **45**, 5.
3 E. G. Steward, B. P. Cook and E. A. Kellett, *Nature*, 1960, **187**, 2.
4 A. Allain, J. Kang, K. Banerjee and A. Kis, *Nat. Mater.*, 2015, **14**, 1195–1205.
5 Y. Wang, R. X. Yang, R. Quhe, H. Zhong, L. Cong, M. Ye, Z. Ni, Z. Song, J. Yang, J. Shi, J. Li and J. Lu, *Nanoscale*, 2016, **8**, 1179–1191.
6 F. Wang, J. Wang, S. Guo, J. Zhang, Z. Hu and J. Chu, *Sci. Rep.*, 2017, **7**, 44712.
7 N. Kaushik, A. Nipane, F. Basheer, S. Dubey, S. Grover, M. M. Deshmukh and S. Lodha, *Appl. Phys. Lett.*, 2014, **105**, 113505.
8 M. R. Laskar, D. N. Nath, L. Ma, E. W. Lee, C. H. Lee, T. Kent, Z. Yang, R. Mishra, M. A. Roldan, J.-C. Idrobo, S. T. Pantelides, S. J. Pennycook, R. C. Myers, Y. Wu and S. Rajan, *Appl. Phys. Lett.*, 2014, **104**, 092104.
9 K. Sano, T. Takahashi and K. Uchida, *Jpn. J. Appl. Phys.*, 2016, **55**, 036501.
10 Y. Liu, J. Guo, E. Zhu, L. Liao, S. J. Lee, M. Ding, I. Shakir, V. Gambin, Y. Huang and X. Duan, *Nature*, 2018, **557**, 696–700.
11 M. Fontana, T. Deppe, A. K. Boyd, M. Rinzan, A. Y. Liu, M. Paranjape and P. Barbara, *Sci. Rep.*, 2013, **3**, 1634.

12 C. D. English, G. Shine, V. E. Dorgan, K. C. Saraswat and E. Pop, *Nano Lett.*, 2016, **16**, 3824–3830.
13 G. Giovannetti, P. A. Khomyakov, G. Brocks, V. M. Karpan, J. van den Brink and P. J. Kelly, *Phys. Rev. Lett.*, 2008, **101**, 026803.
14 M. Buscema, G. A. Steele, H. S. J. van der Zant and A. Castellanos-Gomez, *Nano Res.*, 2015, **7**, 561–571.
15 Y. Li, Z. Qi, M. Liu, Y. Wang, X. Cheng, G. Zhang and L. Sheng, *Nanoscale*, 2014, **6**, 15248–15254.
16 C. K. Gan and Y. Y. F. Liu, *Phys. Rev. B*, 2016, **94**, 134303.
17 S. McDonnell, R. Addou, C. Buie, R. M. Wallace and C. L. Hinkle, *ACS Nano*, 2014, **8**, 9.
18 M. Currie, A. T. Hanbicki, G. Kioseoglou and B. T. Jonker, *Appl. Phys. Lett.*, 2015, **106**, 201907.
19 S. Tongay, J. Zhou, C. Ataca, J. Liu, J. S. Kang, T. S. Matthews, L. You, J. Li, J. C. Grossman and J. Wu, *Nano Lett.*, 2013, **13**, 2831–2836.
20 X. H. Wang, J. Q. Ning, Z. C. Su, C. C. Zheng, B. R. Zhu, L. Xie, H. S. Wu and S. J. Xu, *RSC Adv.*, 2016, **6**, 27677–27681.
21 S. Bettis Homan, V. K. Sangwan, I. Balla, H. Bergeron, E. A. Weiss and M. C. Hersam, *Nano Lett.*, 2016, **17**, 164–169.
22 R. Xu, J. Yang, Y. Zhu, H. Yan, J. Pei, Y. W. Myint, S. Zhang and Y. Lu, *Nanoscale*, 2016, **8**, 129–135.
23 Z. Yin, H. Li, H. Li, L. Jiang, Y. Shi, Y. Sun, G. Lu, Q. Zhang, X. Chen and H. Zhang, *ACS Nano*, 2012, **6**, 7.
24 A. Sharma, B. Wen, B. Liu, Y. W. Myint, H. Zhang and Y. Lu, *Small*, 2018, e1704556.
25 Y. Gong, J. Lin, X. Wang, G. Shi, S. Lei, Z. Lin, X. Zou, G. Ye, R. Vajtai, B. I. Yakobson, H. Terrones, M. Terrones, B. K. Tay, J. Lou, S. T. Pantelides, Z. Liu, W. Zhou and P. M. Ajayan, *Nat. Mater.*, 2014, **13**, 1135–1142.
26 L. Zhang, A. Sharma, Y. Zhu, Y. Zhang, B. Wang, M. Dong, H. T. Nguyen, Z. Wang, B. Wen, Y. Cao, B. Liu, X. Sun, J. Yang, Z. Li, A. Kar, Y. Shi, D. Macdonald, Z. Yu, X. Wang and Y. Lu, *Adv. Mater.*, 2018, e1803986.
27 Y. C. Lin, R. K. Ghosh, R. Addou, N. Lu, S. M. Eichfeld, H. Zhu, M. Y. Li, X. Peng, M. J. Kim, L. J. Li, R. M. Wallace, S. Datta and J. A. Robinson, *Nat. Commun.*, 2015, **6**, 7311.
28 X. Hong, J. Kim, S. F. Shi, Y. Zhang, C. Jin, Y. Sun, S. Tongay, J. Wu, Y. Zhang and F. Wang, *Nat. Nanotechnol.*, 2014, **9**, 682–686.
29 J. S. Ross, S. Wu, H. Yu, N. J. Ghimire, A. M. Jones, G. Aivazian, J. Yan, D. G. Mandrus, D. Xiao, W. Yao and X. Xu, *Nat. Commun.*, 2013, **4**, 1474.
30 K. F. Mak, K. He, C. Lee, G. H. Lee, J. Hone, T. F. Heinz and J. Shan, *Nat. Mater.*, 2013, **12**, 207–211.
31 J. Pei, J. Yang, R. Xu, Y. H. Zeng, Y. W. Myint, S. Zhang, J. C. Zheng, Q. Qin, X. Wang, W. Jiang and Y. Lu, *Small*, 2015, **11**, 6384–6390.
32 W. Liu, J. Kang, D. Sarkar, Y. Khatami, D. Jena and K. Banerjee, *Nano Lett.*, 2013, **13**, 1983–1990.
33 F. Xia, V. Perebeinos, Y. M. Lin, Y. Wu and P. Avouris, *Nat. Nanotechnol.*, 2011, **6**, 179–184.
34 M. Florian, M. Hartmann, A. Steinhoff, J. Klein, A. W. Holleitner, J. J. Finley, T. O. Wehling, M. Kaniber and C. Gies, *Nano Lett.*, 2018, **18**, 2725–2732.
35 D. Somvanshi, S. Kallatt, C. Venkatesh, S. Nair, G. Gupta, J. K. Anthony, D. Karmakar and K. Majumdar, *Phys. Rev. B*, 2017, **96**, 205423.
36 X. Wen, A. Sitt, P. Yu, Y. R. Toh and J. Tang, *Phys. Chem. Chem. Phys.*, 2012, **14**, 3505–3512.
37 S. Mouri, Y. Miyauchi and K. Matsuda, *Nano Lett.*, 2013, **13**, 5.